AFRL-AFOSR-UK-TR-2012-0010

Chemistry of Singlet Oxygen [O2(a1DELTAg)] in the Upper Atmosphere

John M. Plane

The University of Leeds
School of Chemistry
Woodhouse Lane
Leeds, United Kingdom LS29JT

February 2012

Final Report for 20 April 2010 to 19 November 2011

Air Force Research Laboratory
Air Force Office of Scientific Research
European Office of Aerospace Research and Development
Unit 4515 Box 14, APO AE 09421

REPORT DOCUMENTATION PAGE

Form Approved OMB No. 0704-0188

1. REPORT DATE *(DD-MM-YYYY)*	2. REPORT TYPE	3. DATES COVERED *(From – To)*
06-February-2012	Final Report	20 April 2010 – 19 November 2011

4. TITLE AND SUBTITLE

Chemistry of Singlet Oxygen [O2(a1DELTAg)] in the Upper Atmosphere

5a. CONTRACT NUMBER

FA8655-10-1-3045

5b. GRANT NUMBER

Grant 10-3045

5c. PROGRAM ELEMENT NUMBER

61102F

6. AUTHOR(S)

Professor John M. Plane

5d. PROJECT NUMBER

5d. TASK NUMBER

5e. WORK UNIT NUMBER

7. PERFORMING ORGANIZATION NAME(S) AND ADDRESS(ES)

The University of Leeds
School of Chemistry
Woodhouse Lane
Leeds, United Kingdom LS2 9JT

8. PERFORMING ORGANIZATION REPORT NUMBER

N/A

9. SPONSORING/MONITORING AGENCY NAME(S) AND ADDRESS(ES)

EOARD
Unit 4515 BOX 14
APO AE 09421

10. SPONSOR/MONITOR'S ACRONYM(S)

AFRL/AFOSR/RSW (EOARD)

11. SPONSOR/MONITOR'S REPORT NUMBER(S)

AFRL-AFOSR-UK-TR-2012-0010

12. DISTRIBUTION/AVAILABILITY STATEMENT

Approved for public release; distribution is unlimited. (approval given by local Public Affairs Office)

13. SUPPLEMENTARY NOTES

14. ABSTRACT

This project completed the following objectives:
-developed a method (based on technique pioneered by Dr A. Viggiano) to produce molecular oxygen in it's first electronically excited state
-produced an absolute calibration of the O2(a) concentration which showed the yield of O2(a) from the Cl2 generator ranged from 16 to 26%
-studied the reaction kinetics at 300 K of atomic Mg, Ca and Fe with O2(a) in a fast flow tube, where the metal atoms were produced either by thermal evaporation (Mg and Ca) or pulsed laser ablation (Fe), and then detected by laser induced fluorescence
- carried out high level electronic structure calculations to explore the potential energy surfaces for these metal atom + O2(a) reactions, as well as the reaction SiO + O2(a)
Conclusions include:
-the reaction Ca + O2(a) mostly occurs via recombination to produce CaO2(1A1), with a rate coefficient that is ~80 times larger than for the reaction Ca + O2(X). There is also limited switching through a conical intersection between singlet and triplet surfaces, leading to the bimolecular products CaO + O
-the reaction Mg + O2(a) occurs exclusively by recombination on a singlet surface, producing MgO2(1A1). The rate coefficient is ~4000 times larger than for the reaction Mg + O2(X). However, there are no surface crossings between the initial singlet and lower-lying triplet surfaces
-the reaction Fe + O2(a) produces FeO + O, although with a probability of only ~ 0.1%. There is no evidence for recombination, suggesting that this reaction proceeds mostly by near-resonant electronic energy transfer, producing O2(X) and Fe(a5F) (the lowest-lying excited state of Fe)
-the reaction SiO + O2(a) has a significant barrier of 55 kJ mol-1 and also requires a singlet-triplet surface crossing in order to produce SiO2 + O
-the reaction Si(cation) + O2(a) is the most important removal process for Si cations in the daytime atmosphere between 85 and 107 km
-the reaction of Ca with O2(a) is a factor of ~4 times slower than the reaction of Ca with O3, during daytime between 85 and 110 km
- the reactions of Fe, Si, SiO and Mg with O2(a) are too slow to be atmospherically significant

15. SUBJECT TERMS

EOARD, Atmospheric Physics, Chemistry

16. SECURITY CLASSIFICATION OF:			17. LIMITATION OF ABSTRACT	18, NUMBER OF PAGES	19a. NAME OF RESPONSIBLE PERSON
a. REPORT	b. ABSTRACT	c. THIS PAGE			Brad Thompson
UNCLAS	UNCLAS	UNCLAS	SAR	19	19b. TELEPHONE NUMBER *(Include area code)* +44 (0)1895 616163

European Office of Aerospace Research and Development: award no. FA8655-10-1-3045

FINAL Report

Project Title: Chemistry of singlet Oxygen [$O_2(a^1\Delta_g)$] in the Upper Atmosphere

Start date: **20 April 2010** **End date**: **19 November 2011**

Organization: **University of Leeds**

Principal investigator: **Professor John M C Plane**
Contact details: School of Chemistry, University of Leeds
Leeds LS2 9JT, United Kingdom
Tel: (44) 113 3438044
Fax: (44) 113 3436401
Email: j.m.c.plane@leeds.ac.uk

Professor J. M. C. Plane
Principal Investigator

Date: 6th Feburary 2012

Summary

The following objectives have been achieved:

- developed a method for producing molecular oxygen in its first electronically excited state (designated $O_2(a^1\Delta_g)$), based on the technique pioneered by Dr A. A. Viggiano at AFRL
- produced an absolute calibration of the $O_2(a)$ concentration using 1270 nm emission from $O_2(a^1\Delta_g - {}^3\Sigma_g^-)$; the yield of $O_2(a)$ from Cl_2 in the generator ranged from 16 to 26%
- studied the reaction kinetics at 300 K of atomic Mg, Ca and Fe with $O_2(a)$ in a fast flow tube, where the metal atoms were produced either by thermal evaporation (Mg and Ca) or pulsed laser ablation (Fe), and then detected by laser induced fluorescence
- carried out high level electronic structure calculations to explore the potential energy surfaces for these metal atom + $O_2(a)$ reactions, as well as the reaction SiO + $O_2(a)$

Conclusions:

- the reaction Ca + $O_2(a)$ mostly occurs via recombination to produce $CaO_2(^1A_1)$, with a rate coefficient that is ~80 times larger than for the reaction Ca + $O_2(X)$. There is also limited switching through a conical intersection between singlet and triplet surfaces, leading to the bimolecular products CaO + O
- the reaction Mg + $O_2(a)$ reaction occurs exclusively by recombination on a singlet surface, producing $MgO_2(^1A_1)$. The rate coefficient is ~4000 times larger than for the reaction Mg + $O_2(X)$. However, there are no surface crossings between the initial singlet and lower-lying triplet surfaces
- the reaction Fe + $O_2(a)$ produces FeO + O, although with a probability of only ~ 0.1%. There is no evidence for recombination, suggesting that this reaction proceeds mostly by near-resonant electronic energy transfer, producing $O_2(X)$ and $Fe(a^5F)$ (the lowest-lying excited state of Fe)
- the reaction SiO + $O_2(a)$ has a significant barrier of 55 kJ mol^{-1} and also requires a singlet-triplet surface crossing in order to produce SiO_2 + O
- the reaction Si^+ + $O_2(a)$ (measured by Dr Viggiano at AFRL) is the most important removal process for Si^+ ions in the daytime atmosphere between 85 and 107 km
- the reaction of Ca with $O_2(a)$ is a factor of ~4 times slower than the reaction of Ca with O_3, during daytime between 85 and 110 km
- the reactions of Fe, Si, SiO and Mg with $O_2(a)$ are too slow to be atmospherically significant.

Publications arising from the project:

Eyet, N., R. J. Bemish, A. A. Viggiano, and J. M. C. Plane (2010), Mesospheric implications for the reaction of Si^+ with $O_2(a\ ^1\Delta_g)$, *Geophys. Res. Lett., 37*, art. no.: L20801.

Plane, J. M. C., C. L. Whalley, L. Soriano, D. Glowacki, A. Goddard and A. A. Viggiano, Reaction kinetics of Ca, Mg and Fe with $O_2(a\ ^1\Delta_g)$, *J. Phys. Chem. A*, to be submitted spring 2012.

1. Introduction

The first excited state of molecular oxygen, $O_2(a^1\Delta_g)$, is produced in the mesosphere-lower thermosphere (MLT) region by photolysis of O_3 at wavelengths shorter than 320 nm:

$$O_3 + h\nu \rightarrow O(^1D) + O_2(a^1\Delta_g)$$

$O_2(a^1\Delta_g)$ is comparatively long-lived in the MLT. The quenching life-time is more than 4 hours, much longer than the phosphorescence lifetime of 72 minutes for emission at 1.27 μm in the infra-red. Since the rate of O_3 photolysis in the MLT is ~8 x 10^{-3} s^{-1}, then during daytime the steady-state ratio $[O_2(a^1\Delta_g)]/[O_3]$ is about 30 [*Brasseur and Solomon*, 2005] and the daytime concentration of $O_2(a^1\Delta_g)$ around 90 - 100 km is ~ 5 x 10^9 cm^{-3} [*Batista et al.*, 1996]. After sunset $O_2(a^1\Delta_g)$ decays by an order of magnitude every 2.8 hours. $O_2(a^1\Delta_g)$ contains almost 1 eV of electronic excitation compared with ground-state $O_2(X^3\Sigma_g^-)$, and thus has the potential to be significantly more reactive, although it is not a radical species.

The purpose of this project was to explore the impact of $O_2(a^1\Delta_g)$ on the constituents of the MLT which are produced by meteoric ablation. The interactions of metallic and silicon species with $O_2(a^1\Delta_g)$ have not before been studied (to the best of our knowledge). However, following the recent development of a new method for producing $O_2(^1\Delta_g)$ cleanly and at significant concentrations [*Midey et al.*, 2008], such a study has become feasible. The work was undertaken in collaboration with the research group of Dr A. A. Viggiano (Air Force Research Laboratory, Space Vehicles Directorate), who pioneered this new technique of producing $O_2(a^1\Delta_g)$ for laboratory kinetic studies [*Midey et al.*, 2009].

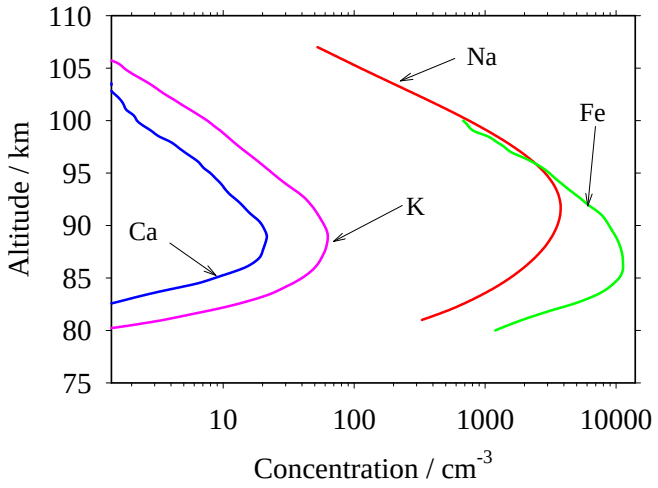

Figure 1. Vertical profiles of the annual mean concentrations at northern hemisphere mid-latitudes of: Na (Plane, J. M. C. et al. *J. Geophys. Res.* **104**, 3773-3788, 1999); Fe (Helmer, M. et al. *J. Geophys. Res.* **103**, 10913-10925, 1998.); K (Eska, V. et al. *J. Geophys. Res.* **104**, 17173-17186, 1999); and Ca (Gerding, M. et al. *J. Geophys. Res.* **105**, 27131-27146, 2000).

The major source of metals in the earth's upper atmosphere is the ablation of the roughly 50 tonnes of interplanetary dust that enters each day from space [*Plane*, 2003]. This gives rise to the permanent layers of metal atoms that occur globally in the MLT region between about 75 and 110 km (Figure 1). Four metals – Na, Fe, K and Ca – have been studied intensively during the last two decades using the ground-based resonance lidar technique [*Bowman et al.*, 1969; *Eska et al.*, 1999; *Gerding et al.*, 2000; *Kane and Gardner*, 1993]. Metallic (and silicon) ions have been detected by rocket-borne mass spectrometry [*Grebowsky and Aikin*, 2002; *Kopp*, 1997]. Most recently, satellite-borne spectrometric observations of the earth's dayglow have been used to retrieve the global layers of metal atoms and ions, in particular Mg and Mg^+ [*Fan et al.*, 2007; *Scharringhausen et al.*, 2008].

Meteoric ablation injects metal atoms and ions directly into the MLT [*Vondrak et al.*, 2008]. These species then undergo neutral and ion-molecule chemistry. Below 90 km, metal atoms are rapidly oxidised by a series of reactions involving O_3, O_2, H_2O and CO_2 to reservoir species such as oxides, hydroxides and bicarbonates. However, these species react with either atomic O or H (and, to a lesser extent, undergo daytime photolysis) to regenerate metal atoms. Thus, the atomic metal layers only appear above 80 km, where atomic O and H increase by several orders of magnitude and are present

both during day and night [*Plane*, 2003]. This ensures rapid recycling of the metal atoms from their reservoirs. The small scale height of 2 - 3 km (the scale height is the distance over which the concentration changes by a factor of *e*) on the undersides of the layers (Figure 1) closely follows the atomic O fall-off. Below about 85 km the reservoir species are permanently lost by condensation onto meteoric smoke particles. These are approximately 1 nm-size particles which form from the polymerization of metal oxides, carbonates and silicates produced by meteoric ablation [*Bardeen et al.*, 2008; *Hunten et al.*, 1980; *Kalashnikova et al.*, 2000; *Saunders and Plane*, 2006]. Meteoric smoke particles also probably provide ice nuclei for the formation of noctilucent clouds (NLCs) in the summer high-latitude mesosphere [*Bardeen et al.*, 2008; *Megner et al.*, 2006]. The ice particles in these clouds, with radii of ~50 nm, remove metallic species even more efficiently [*Gardner et al.*, 2005; *Plane et al.*, 2004]. Smaller ice particles (5 - 10 nm radius) affect the plasma locally and give rise to very strong radar echoes known as polar mesospheric summer echoes (PMSE) around 85 km [*Megner et al.*, 2006]. NLCs appear increasingly to be a sensitive indicator of climate change in the mesosphere [*Shettle et al.*, 2009].

Above 95 km in the lower *E* region of the ionosphere, there is a marked increase in the concentration of plasma, which consists mostly of NO^+, O_2^+, and electrons [*Plane*, 2003]. Because of their low ionization potentials, metal atoms charge exchange readily with these positive ions to produce metallic ions. Metallic ions then form clusters with N_2, O_2, CO_2 and H_2O to form strongly-bound cluster ions which undergo dissociative recombination with electrons to yield neutral metal atoms. This process is interrupted by atomic O, which tends to reduce cluster ions back to metal ions [*Plane*, 2003]. Fe^+, Mg^+ and Si^+ are the major components of sporadic *E* layers [*Grebowsky and Aikin*, 2002]. These are thin layers of concentrated plasma (essentially metallic ions and electrons) that occur in the lower thermosphere between about 90 and 120 km. They have a significant impact on radio communications, both by facilitating over-the-horizon HF communication and by obscuring space-to-ground communications. The lifetime of a sporadic *E* layer is largely controlled by ion-molecule chemistry, and can vary from several days at 105 km to only a few minutes at 90 km [*Woodcock et al.*, 2006].

2. Specific objectives of the project

The project involved the kinetic study of a set of reactions between various meteoric species and $O_2(a)$. These reactions, which are listed in Table 1, are all exothermic (or very close to thermoneutral), and could thus be rapid and play important roles in the MLT. The reactions are also of fundamental interest for understanding the role of electronic excitation and spin in controlling chemical reactions.

The reaction between Ca and $O_2(a)$ (reaction 1) could provide an alternative daytime route to oxidizing Ca via O_3 [*Helmer et al.*, 1993], although reaction 1 is formally spin-forbidden. Alternatively, recombination to form the most stable isomer of CaO_2 is spin-allowed, and may be considerably faster than the recombination of Ca and ground-state $O_2(X)$, which has a barrier of about 6 kJ mol^{-1} [*Campbell and Plane*, 2001].

Although not specified in the original proposal, we added a study of the reaction between Mg and $O_2(a)$ (reaction 2). This reaction contrasts with reaction 1 because if reaction occurs then it must involve recombination to MgO_2 (this is because the Mg-O bond is relatively weak and so formation of MgO + O is endothermic by 164 kJ mol^{-1} [*Lide*, 2006]). Note that both the Ca and Mg reactions could also quench the $O_2(a)$ to the ground state $O_2(X)$, although this would involve crossing from the reactant singlet surface onto the product triplet surface.

Fe is oxidized to FeO at every collision with O_3 [*Helmer and Plane*, 1994b]. Given that the $[O_2(a)]$ / $[O_3]$ ratio in the mesosphere is ~30, the reaction between Fe and $O_2(a)$ (reaction 3) could therefore substantially increase the daytime oxidation rate of Fe. This reaction could also involve recombination on a quintet surface to yield FeO_2 (or the more stable OFeO isomer). In contrast, the

reaction between Fe and ground-state $O_2(X^3\Sigma_g^-)$ can only produce FeO_2, but has a large electronic barrier of about 17 kJ mol^{-1} [*Helmer and Plane*, 1994a]. Another interesting possibility is near-resonant electronic energy transfer to yield $Fe(a^5F) + O_2(X)$. $Fe(a^5F)$ is the first electronically-excited state of Fe.

Reaction 4 may provide an important route in the mesosphere for oxidizing SiO to SiO_2, which is the most stable form of silicon and a likely precursor of meteoric smoke [*Saunders and Plane*, 2006]. One pathway is the reaction between SiO and O_3: however, we have shown recently that this reaction is very slow [*Gomez Martin et al.*, 2009b], so that reaction 2 could oxidize SiO up to 15,000 times faster, although it would involve a singlet-triplet surface crossing.

During the course of this project, the reaction between Si^+ and $O_2(a)$ (reaction 5) was studied experimentally at AFRL by Dr A A Viggiano's group [*Eyet et al.*, 2010]. The reaction was shown to be relatively fast ($k_5(200\ K) = 4 \times 10^{-11}$ cm^3 $molecule^{-1}$ s^{-1}). The atmospheric implications were then studied as part of this project.

The original proposal also listed the reaction between Si and $O_2(a)$ for study. This reaction is exothermic and spin-allowed, producing $SiO + O(^1D)$ or $SiO(^3\Pi) + O(^3P)$). However, we have shown recently that the reaction between Si and ground-state $O_2(X)$ is fast (($k(200\ K) = 1.3 \times 10^{-10}$ cm^3 $molecule^{-1}$ s^{-1}) [*Gomez Martin et al.*, 2009a], so that the reaction with $O_2(a)$ will have an insignificant effect on the oxidation of Si in the MLT. This reaction was therefore replaced in the project with a study of reaction 2.

Table 1. Reactions of meteoric species with $O_2(a^1\Delta_g)$ that could play important roles in the mesosphere and lower thermosphere

No.	Reaction	ΔH_0 / kJ mol^{-1}	Electron spin conserved?
1	$Ca + O_2(a^1\Delta_g) \rightarrow CaO(^1\Sigma) + O(^3P)$	0 [a]	No
	$\rightarrow CaO_2(^1A_1)$	-279 [b]	Yes
	$\rightarrow Ca + O_2(^3\Sigma_g^-)$	-93 [a]	No
2	$Mg + O_2(a^1\Delta_g) \rightarrow MgO_2(^1A_1)$	-149 [b]	Yes
	$\rightarrow Mg + O_2(^3\Sigma_g^-)$	-93 [a]	No
3	$Fe + O_2(a^1\Delta_g) \rightarrow FeO(^5\Sigma) + O(^3P)$	-2±8	Yes
	$\rightarrow FeO_2(^5A_1)$	-376 [c]	Yes
	$\rightarrow Fe(a^5F_2) + O_2$	0 [a]	Yes
	$\rightarrow Fe(a^5D) + O_2$	-94 [a]	Yes
4	$SiO + O_2(a^1\Delta_g) \rightarrow SiO_2 + O(^3P)$	-31 [b]	No
	$\rightarrow OSiO_2(^1A_1)$	-273 [b]	Yes
5	$Si^+ + O_2(a^1\Delta_g) \rightarrow SiO^+ + O$	-67 [b]	Yes

[a] Using experimental energies [*Lide*, 2006]. [b] Calculated at the CBS-Q level of theory [*Frisch et al.*, 2009]; [c] Calculated at the B3LYP/6-311+g(2d,p) level of theory [*Frisch et al.*, 2009]

3. Experimental technique

Figure 2 is a schematic diagram of the fast flow tube apparatus that was used to study the kinetics of the Ca, Mg and Fe reactions. The stainless steel flow tube has an internal diameter of 37.5 mm and consists of sections of tube, cross-pieces and nipple sections connected by conflat flanges sealed with copper gaskets. The tube has a total length of 1130 mm from the upstream entry point of the carrier gas to the downstream laser induced fluorescence (LIF) detection cell. Calcium atoms were produced continuously by heating calcium pellets (Aldrich, 99 %) to 1070 - 1120 K. Magnesium atoms were produced by heating magnesium pellets (Aldrich, 99.5 %) to a temperature between 700 and 800 K. The pellets were located in an aluminium oxide crucible placed inside a tungsten basket heater, positioned 1120 mm upstream of the LIF cell. The Ca or Mg atoms were entrained in the main carrier flow of N_2, which entered the tube upstream of the crucible. Ca was detected by LIF at 422.7 nm ($Ca(4^1P_1 - 4^1S)$) using a Nd-YAG-pumped dye laser (pulse rate 10 Hz; pulse energy 10 mJ). Mg was detected by LIF at 285.2 nm ($Mg(3^1P_1 – 3^1S_0)$), after frequency-doubling the dye laser using a BBO crystal.

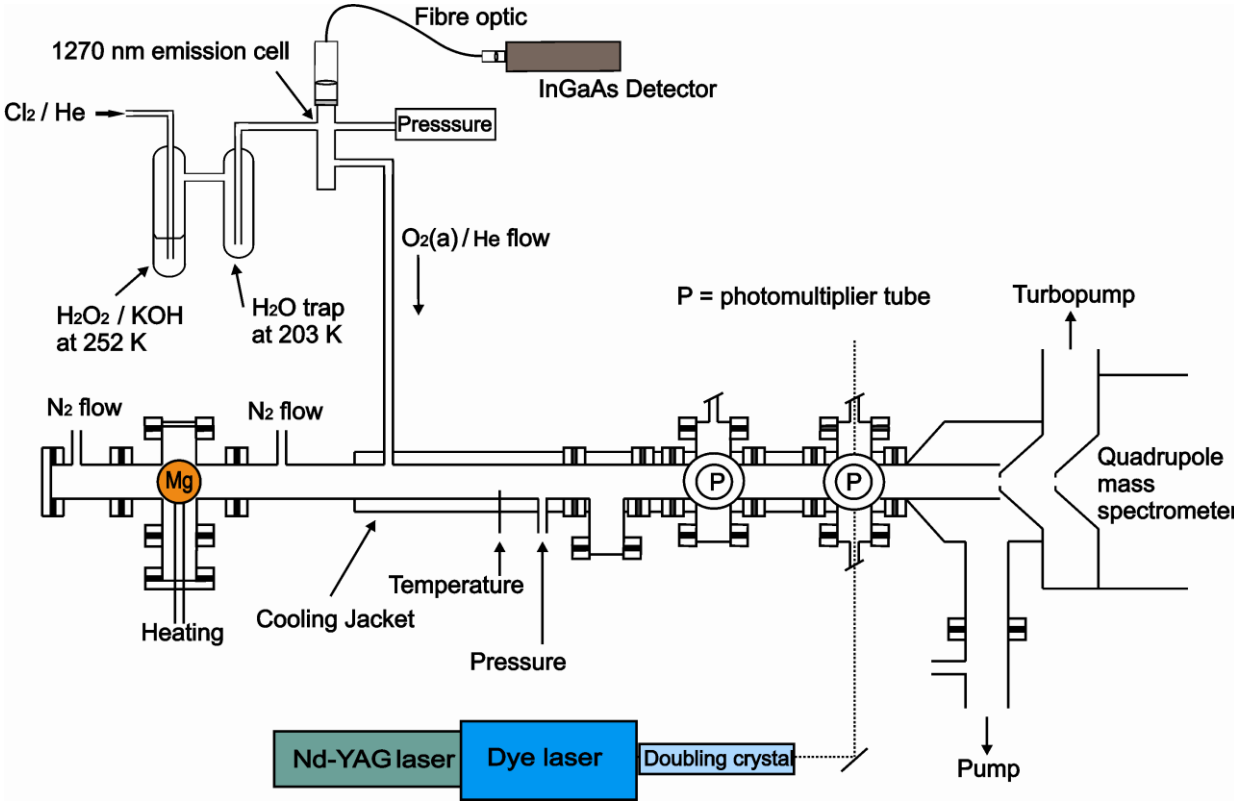

Figure 2. Schematic diagram of the $O_2(a)$ generator coupled to a fast flow with laser induced fluorescence detection for studying metal atom reactions (exemplified by Mg) with $O_2(a^1\Delta_g)$

The source of Fe atoms in the flow tube was the pulsed ablation of a pure iron rod, using a Nd:YAG laser (λ = 532nm, pulse energy = 22 – 31 mJ, repetition rate = 8 Hz). The rod was coupled to a stepper motor (via a vacuum feedthrough in a side-arm of the flow tube), so that the rod could be rotated (2 - 4 Hz) and also translated slowly. This ensured that a fresh surface of the rod was presented to each successive laser shot, in order to keep the resulting pulses of ablated Fe as uniform as possible. The iron rod was long enough ($\approx$ 5 cm) to project across the central axis of the tube. The laser was loosely focused onto the rod through an orthogonal side-arm, so that the point of ablation was in the centre of the flow tube. The pulse of Fe atoms was then entrained in the N_2 carrier gas and transported downstream to the LIF cell, where the Fe was detected by LIF at 248.3 nm $Fe(x^5F^o_5 \leftarrow a^5D_4)$.

The reactant flow ($O_2(a)$ in He) was injected via a side port downstream of the crucible (Figure 2). The gas flow exited the tube through a throttle valve to a booster pump backed by a rotary pump, providing a volume displacement rate of 110 l s^{-1}. Typically, a total gas flow rate of 3200 sccm was used with pressures ranging from 1 to 10 Torr. The Reynolds number was always below 80, ensuring laminar flow within the tube.

$O_2(a^1\Delta_g)$ was prepared using the technique pioneered by Viggiano's group [*Midey et al.*, 2008; *Midey et al.*, 2007; *Midey et al.*, 2009], where Cl_2 is bubbled through a chilled alkaline solution of H_2O_2:

$$Cl_{2\,(g)} + H_2O_{2\,(aq)} + 2KOH_{(aq)} \rightarrow O_2(a^1\Delta_g) / O_2(X^3\Sigma_g^-)_{(g)} + 2KCl_{(aq)} + H_2O \qquad (6)$$

This produces $O_2(a^1\Delta_g)$ at up to 30% yield [*Midey et al.*, 2008]. The $O_2(a)$ generator constructed for this project is illustrated schematically in Figure 2. The two traps and the cell used to monitor emission at 1270 nm from $O_2(a)$ were contructed from Pyrex glass. The first trap is where reaction 6 takes place. This trap, containing 60 ml of 35% w/w H_2O_2, was held at -21^{o}C (provided by a water ice, dry ice and NaCl slush). Using a burette, 40 ml of chilled 4.04 M KOH was added, and the trap was then attached to the rest of the generator. A 10% Cl_2/He was then bubbled through the resulting slush, at flow rates up to 100 sccm. The second trap, held at -70^{o}C (using a 30% H_2O/CH_3OH slush), was used to dry the gas flow by freezing out H_2O. The O_2/He flow then entered the cylindrical optical emission cell (length = 100 mm, radius = 10 mm), before flowing through a Teflon valve into the fast flow tube.

The weak emission at 1270 nm from $O_2(a\text{-}X)$ emission, exiting through a window at one end of the cell, was focused by a lens (bi-convex BK-7 lens, f = 30 mm)) through an interference filter (centre wavelength = 1270 nm, FWHM = 4.2 nm, peak transmission = 33%) into a glass fibre optic bundle of length 610 mm (Figure 2). The light exiting the bundle was then focused by a second lens onto an InGaAs photodiode detector (Oriel, Model 71671). The photodiode current was read by a pico-ammeter (Keithley). The absolute sensitivity of this optical assembly – light collection, transmission through the fibre optic, and detection – was calibrated using a radiometric calibration standard (Ocean Optics LS-1-CAL NIST-traceable light source).

Experimental Results

Calibration of the $O_2(a)$ flow

Figure 3 shows that the InGaAs photodiode current resulting from 1270 nm emission in the optical cell was always proportional to the Cl_2 concentration entering the first trap of the $O_2(a)$ generator. This implies that a constant fraction of the O_2 produced by reaction 6 was in the $a^1\Delta_g$ state. The calibration of the absolute $O_2(a)$ concentration was achieved in two stages:

1. A computer ray-tracing model was developed to calculate the total collection efficiency of 1270 nm photons emitted in the gas cell. This model assumes that $O_2(a)$ has a uniform concentration in the emission cell, which should be the case given its long lifetime (τ_{rad} = 4200 s; quenching in He is negligible). The model then determines the probability of a photon emitted at each point in the cell being captured by the bi-convex lens and focused through the interference filter onto the entrance of the fibre optic bundle. The total number of photons entering the bundle is then computed by integrating over the cell volume. A correction is then applied because the $O_2(a\text{-}X)$ vibrational band structure is significantly broader that the bandpass of the interference filter: only 20.1% of the total emission spectral intensity falls within the filter bandpass. The result is that if the concentration of $O_2(a)$ in the cell were 1.0×10^{16} cm^{-3}, then the $O_2(a\text{-}X)$ emission power entering the fibre bundle would be 0.12 nW.

2. With the light collecting system removed from the optical emission cell, the photodiode current was measured as a function of the distance between the radiometric calibration standard and the collection lens. This showed that the calibration factor was 103 pA nW^{-1}. Hence, a concentration of

1.0×10^{16} cm^{-3} O_2(a) in the cell would produce a photodiode current of 12.4 pA. That is, the calibration factor was 8.1×10^{14} cm^{-3} pA^{-1}.

The right-hand ordinate in Figure 3 shows the resulting O_2(a) concentrations, calculated by applying this calibration factor to the detector current on the left-hand ordinate. The selection of experimental runs shown in Figure 3 covers the range of conversion efficiencies of Cl_2 into O_2(a) observed during the project, which ranged from 16 to 26%. This variation in efficiency seemed most likely due to the cleanliness of the Pyrex glass traps.

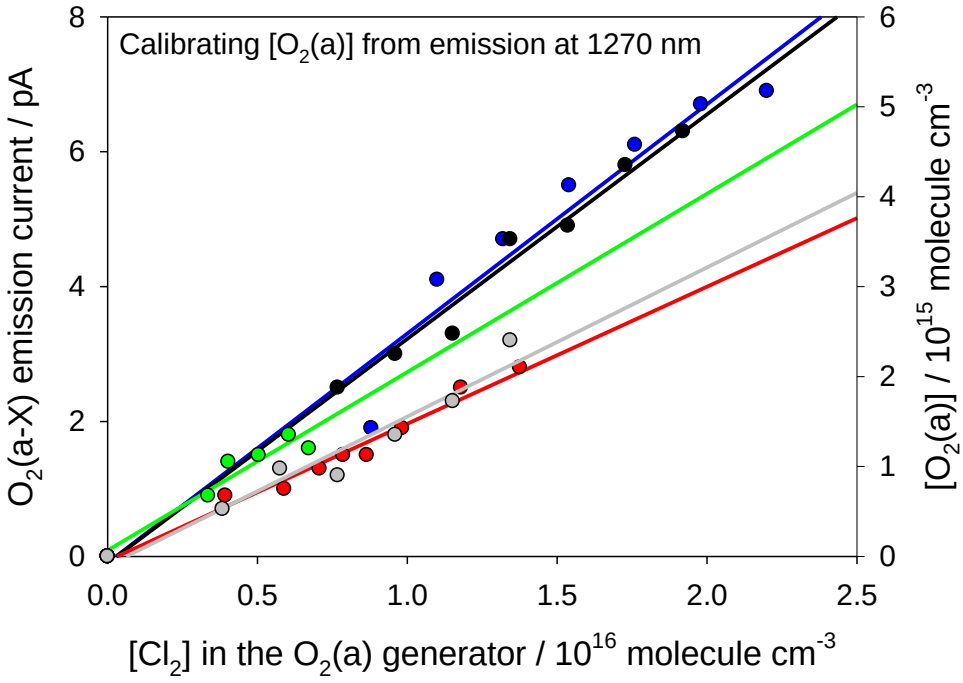

Figure 3. O_2(a) emission current measured with the In-Ga-As detector at 1270 nm, as a function of [Cl_2] in the generator. The corresponding calibrated [O_2(a)] is shown on the right-hand ordinate. Data from a selection of experimental runs over several months shows that the efficiency for O_2(a) production ranged from 16 – 26% of the Cl_2.

Kinetic experiments

Reaction rate coefficients were determined using a procedure we have described in detail elsewhere [*Broadley et al.*, 2007]. Taking reaction 1 as an example, the loss of Ca by diffusion to the flow tube walls and reaction with O_2(a), can be described by a first-order decay coefficient, k', since [O_2(a)] >> [Ca]:

$$k' = k_{\text{diff,Ca}} + k[O_2(a)] \qquad \text{(I)}$$

where $k_{\text{diff,Ca}}$ describes the loss of Ca by diffusion and k is the rate coefficient for reaction 1 (which may depend on pressure). An experiment is carried out by varying [O_2(a)] while keeping the total mass flow rate and pressure in the flow tube constant. This means that $k_{\text{diff,Ca}}$ is constant, as well as the reaction time t between the point of injection of the O_2(a) and the downstream LIF cell. Since the removal of Ca is pseudo first-order,

$$\frac{\ln\left(\dfrac{[\text{Ca}]_0^t}{[\text{Ca}]_{\text{O}_2(a)}^t}\right)}{t} = \frac{\ln[\text{Ca}]_{\text{rel}}}{t} = k[\text{O}_2(a)] \qquad \text{(II)}$$

where $[Ca]_0^t$ is the concentration at the LIF detection cell in the absence of $O_2(a)$, $[Ca]_{O_2(a)}^t$ is the Ca concentration at the LIF detection cell when $O_2(a)$ is added, and $[Ca]_{rel}$ is the ratio of these concentrations. Plots of $\ln[Ca]_{rel} / t$ versus $[O_2(a)]$ are shown in Figure 4, for a range of pressures in the flow tube. The linear dependence expected from equation II is observed, and the slope of each plot gives the second-order rate coefficient *k*.

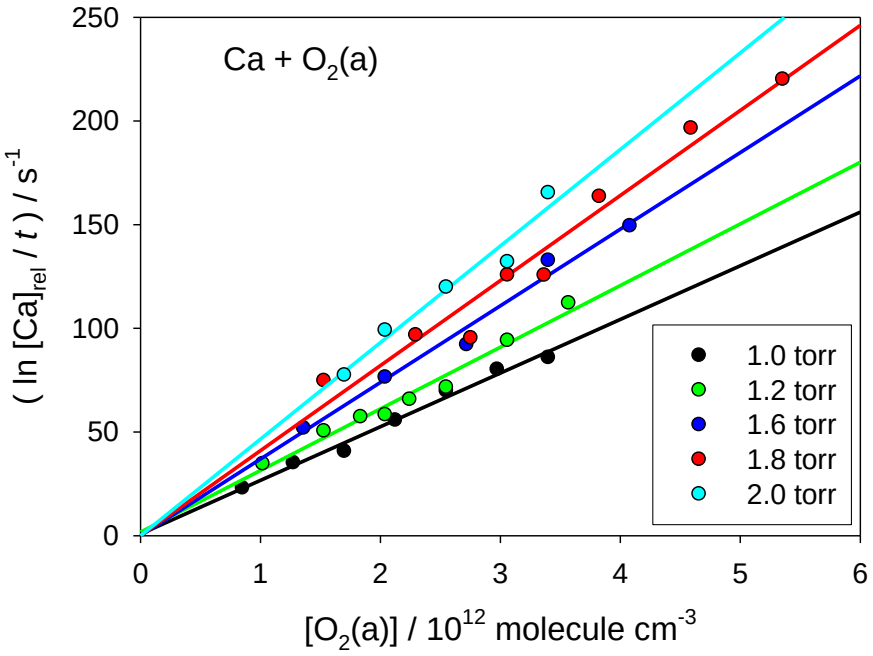

Figure 4. Kinetic plots showing the first-order removal rate of Ca as a function of $[O_2(a)]$, at five different pressures of N_2 in the flow tube.

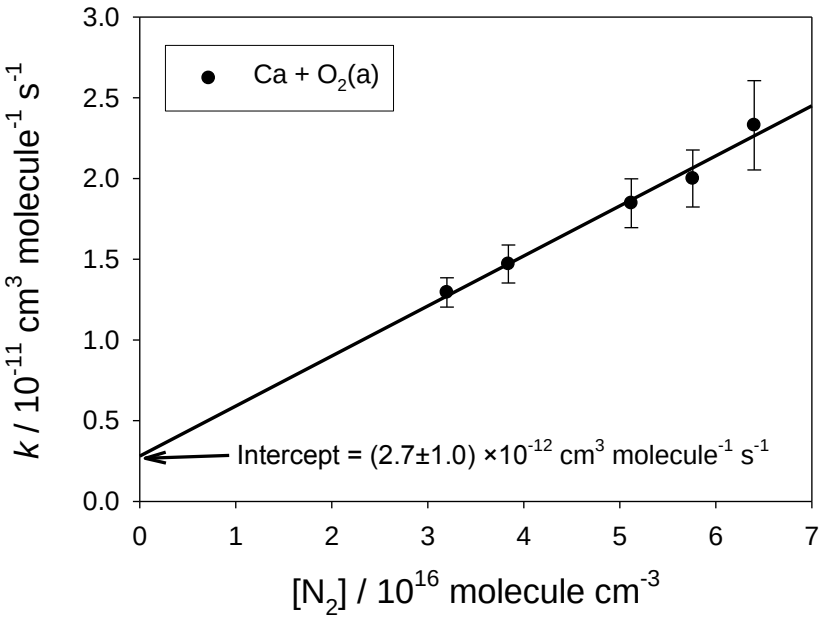

Figure 5. Plot of the second-order rate coefficient for Ca + $O_2(a)$ as a function of N_2 concentration. This reaction exhibits third-order (pressure) dependence demonstrating the formation of $CaO_2(^1A_1)$; the significant intercept indicates that the bimolecular channel to CaO + O is also active.

Figure 4 shows that reaction 1 is pressure dependent. This is confirmed in Figure 5, which is a plot of *k* against $[N_2]$. The slope of this plot yields the third-order rate coefficient listed in Table 1. Note that there is also a significant intercept in Figure 4, which indicates that there is a second-order component to reaction 1.

Figure 6 shows the first-order removal of Fe as a function of [O_2(a)], at two pressures. Note that reaction 3 is clearly independent of pressure. This is confirmed in Figure 7, which also shows the second-order removal rate coefficient for reaction 2 between Mg and O_2(a). The Mg reaction is clearly pressure-dependent although, in contrast to reaction 1 (figure 5), there is not a significant intercept on the ordinate. The rate coefficients for reactions 2 and 3 are also listed in Table 2.

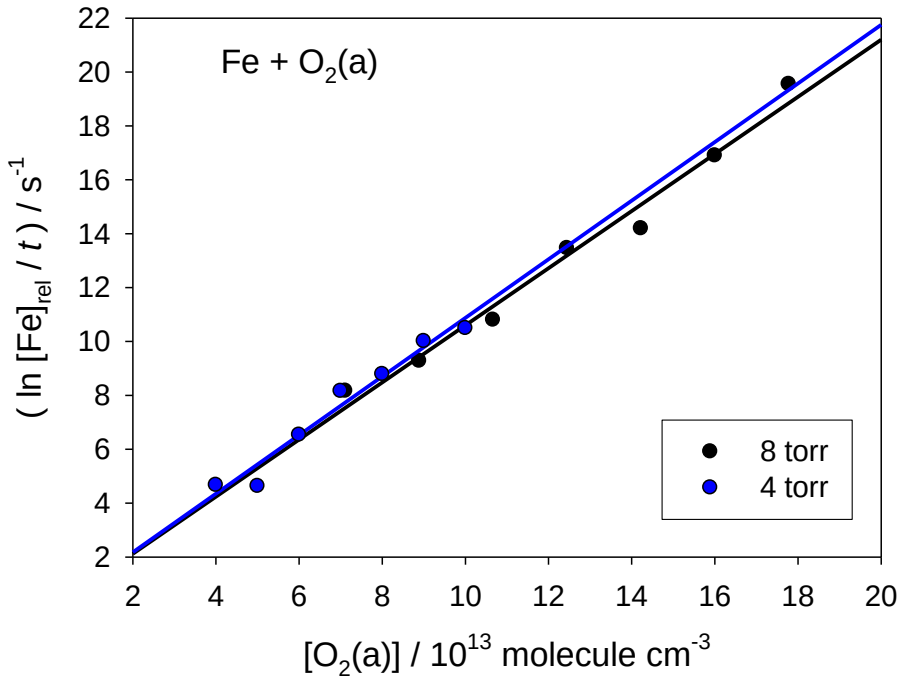

Figure 6. Kinetic plots showing the first-order removal rate of Fe as a function of [O_2(a)], at two different pressures of N_2 in the flow tube.

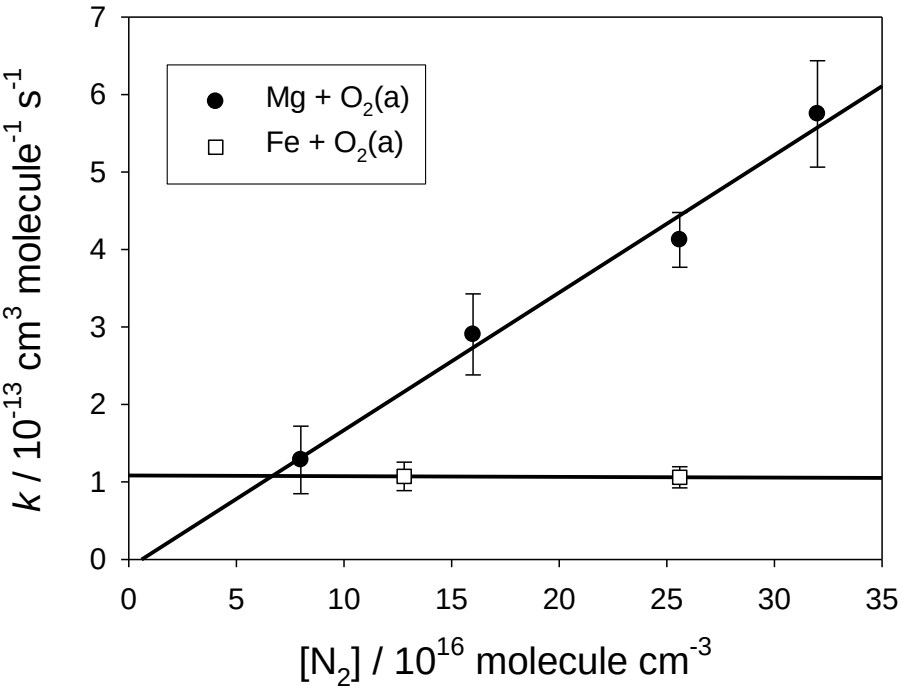

Figure 7. Plot of the second-order rate coefficient for Mg + O_2(a) and Fe + O_2(a) as a function of [N_2]. The Mg reaction exhibits third-order kinetics forming $MgO_2(^1A_1)$. The Fe reaction shows no pressure dependence, indicating the formation of FeO + O is the only reactive channel.

Table 2. Rate coefficients measured in the present study at 296 K. The quoted uncertainties are the standard errors from kinetics plots such as Figures 4 and 6. The total uncertainty, which mostly arises from the systematic uncertainty in the $O_2(a)$ concentration, is estimated to be ±40%.

Reaction	Bimolecular Rate Coefficient cm^3 $molecule^{-1}$ s^{-1}	Termolecular Rate Coefficient cm^6 $molecule^{-2}$ s^{-1}
$Mg + O_2(a)$	$< 2.4 \times 10^{-14}$	$(1.8\pm0.2) \times 10^{-30}$
$Ca + O_2(a)$	$(2.7\pm1.0) \times 10^{-12}$	$(2.9\pm0.2) \times 10^{-28}$
$Fe + O_2(a)$	$(1.1\pm0.1) \times 10^{-13}$	$< 2.4 \times 10^{-31}$

A final point to note here is that Ca, Mg and Fe react comparatively slowly with $O_2(X)$ [*Campbell and Plane*, 2001; *Helmer and Plane*, 1994a; *Nien et al.*, 1993]. Therefore, even though the ratio of $O_2(a)/O_2(X)$ entering the flow tube was in some experimental runs as low as 16%, the reactions of these metal atoms with $O_2(X)$ would have had a negligible impact on their removal rates and hence determination of the $O_2(a)$ kinetics.

Discussion

The recombination reactions of Ca and Mg with $O_2(a)$ are 82 and 4020 times faster, respectively, than their reactions with ground-state $O_2(X)$. In order to understand these striking differences in reactivity, we have used electronic structure (quantum chemistry) calculations, combined with Rice-Ramsperger-Kassell-Markus (RRKM) theory (using the inverse Laplace transform method to solve the Master equation [*Campbell and Plane*, 2001]). Some of this work was done in collaboration with Dr David Glowacki of Bristol University.

Figure 8 illustrates the stationary points on the singlet potential energy surface for $Ca + O_2(a)$ (red lines), as well as the triplet surface (black lines) which links $Ca + O_2(X)$ with the bimolecular products $CaO + O(^3P)$. The hybrid density functional / Hartree-Fock B3LYP method was employed from within the Gaussian 09 suite of programs [*Frisch et al.*, 2009], combined with the 6-311+G(2d,p) triple zeta basis set.. This is a large, flexible basis set which has both polarization and diffuse functions added to the atoms. At this level of theory, the expected uncertainty in the calculated reaction enthalpies is ±20 kJ mol^{-1}. If reaction 1 remains on the singlet surface then the outcome is recombination to form $CaO_2(^1A_1)$, a deep well which is 279 kJ mol^{-1} below the reactants. RRKM theory models successfully the surprisingly fast measured rate coefficient (Table 1) using the calculated vibrational frequencies and rotational constants for CaO_2, and assuming sensible values for the collisional energy removal by N_2. The reaction $Ca + O_2(X)$ is much slower because there is a small barrier (~6 kJ mol^{-1}) in the entrance channel and the well-depth of $CaO_2(^3A_2)$ is much shallower [*Campbell and Plane*, 2001], as shown in Figure 8.

The other interesting feature about reaction 1 is the bimolecular channel, which must correspond to the formation of CaO + O, which involves a spin hop from the singlet to triplet surface. In an effort to characterize the regions of most likely spin hopping within the CaO_2 addition complex, we carried out a number of relaxed multireference CASSCF scans along the O–Ca–O angle. All calculations were performed with a 10 electron, 7 orbital active space. The orbital active space consisted of: (1) the in-plane π and π^* orbitals on O_2; (2) the out-of-plane π and π^* orbitals on O_2; (3) the in-plane O_2 σ and σ^* orbitals; and (4) the dz^2 orbital on Calcium. The results show that the singlet-triplet minimum energy crossing point (MECP) is in the vicinity of the OCaO minimum geometry (right-hand side of Figure 8). In order to avoid convergence problems during the MECP optimization, calculations on both the singlet and triplet surface were carried out without any point group symmetry. The OCaO singlet state was treated using broken spin symmetry in order to capture its diradical character. The results of the MECP optimization yielded a linear OCaO structure with Ca–O bond distances of 1.83 Angstrom. Note that once spin-hopping has occurred, there is a large

barrier on the triplet surface preventing the formation of Ca + O_2(X). Hence, this quenching channel is closed.

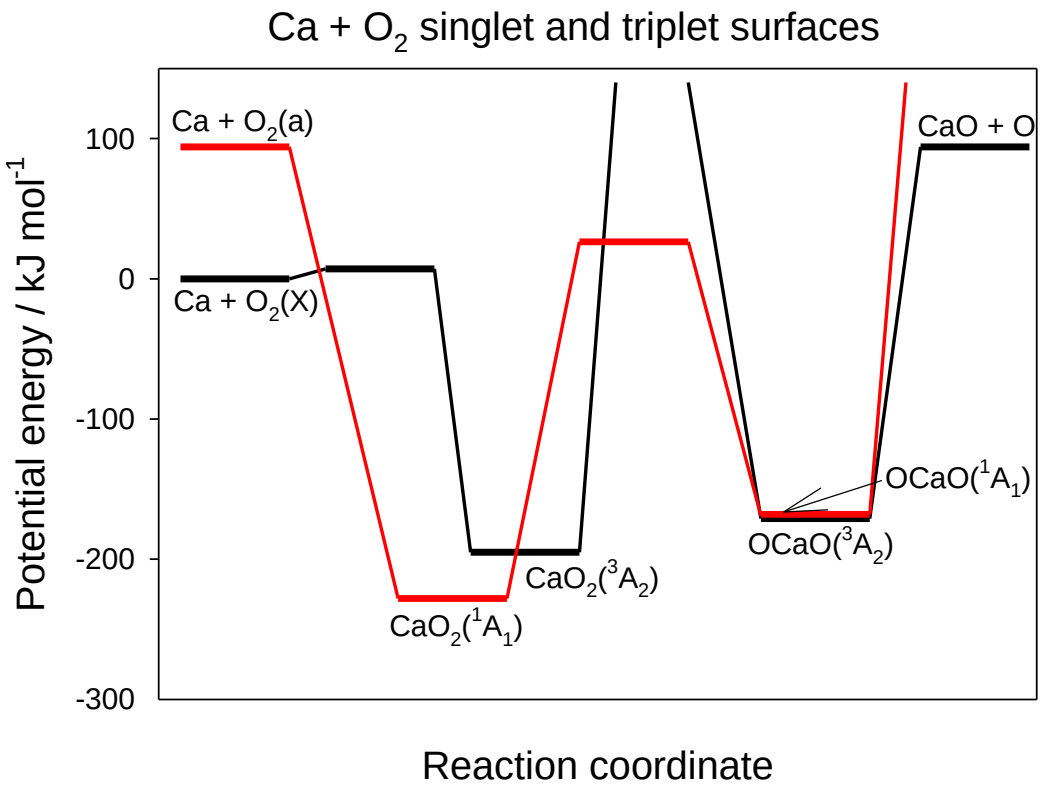

Figure 8. Potential energy curves (calculated at the B3LYP/6-311+g(2d,p) level of theory) for the singlet surface (red lines) and triplet surface (black lines). Recombination of Ca + O_2(a) produces mostly $CaO_2(^1A_1)$. However, there is a conical intersection between $OCaO(^1A_1)$ and $OCaO(^3A_2)$, where there is a small probability of switching onto the triplet surface and generating the bimolecular products CaO + $O(^3P)$.

For reaction 2, recombination to form $MgO_2(^1A_1)$ is the only possible product. The well depth is 149 kJ mol^{-1} below the reactants, and the measured rate coefficient (Table 1) is straight-forwardly modelled using RRKM theory. The reaction is more than 3 orders of magnitude faster than Mg + O_2(X) because there is a significant barrier of 23 kJ mol^{-1} in the entrance channel of the triplet surface [*Nien et al.*, 1993]. Figure 9 is a mesh plot showing parts of the singlet and triplet surfaces, as a function of the distance between the Mg atom and X (the mid-point between the O atoms), and the Mg-X-O angle. There are no crossing-points between the surfaces, at any point below the reactant energy on the singlet surface. Thus, formation of the more stable $MgO_2(^3A_2)$, or quenching to Mg + O_2(X), are ruled out.

Reaction 3 between Fe and O_2(a) starts on a quintet surface. Because of the complex spin multiplicity of Fe, a detailed theoretical treatment of this reaction involves surfaces of singlet, triplet, quintet and septet multiplicities, which is beyond the scope of this study. $Fe(a^5D) + O_2(^1\Delta)$ and $FeO(^5\Sigma) + O(^3P)$ correlate on a quintet surface, explaining the observation of bimolecular kinetics (Table 1). Initially, reaction 3 involves formation of $FeO_2(^5A_1)$. This can then rearrange to $OFeO(^5B_2)$, before dissociating to FeO + O [*Self and Plane*, 2003]. However, $FeO_2(^5A_1)$ can more easily dissociate to $Fe(a^5F) + O_2$(X). This channel represents near-resonant energy transfer (ΔE = -10 to +4 kJ mol^{-1}, depending on the Fe spin-orbit multiplet), and must be the major product of reaction 3. The excited $Fe(a^5F)$ atoms will be quenched to ground-state $Fe(a^5D)$ in only 6 μs at the lowest pressure of N_2 used in the flow tube [*Mitchell and Hackett*, 1990], so this energy transfer reaction would not be observable as a loss of Fe atoms.

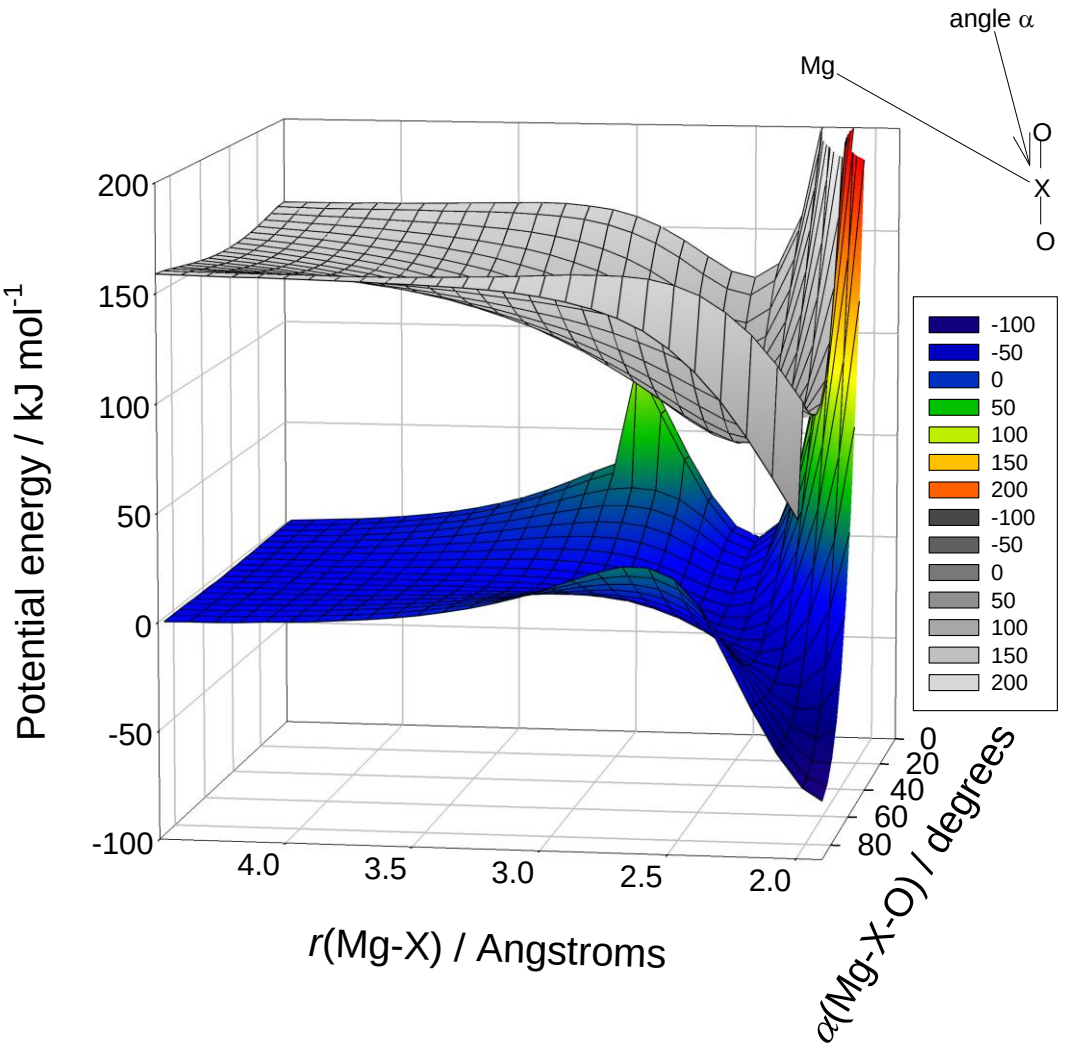

Figure 9. Potential energy surfaces for Mg + O_2(a) (monochrome shading) and Mg + O_2(X) (coloured shading), calculated at the B3LYP/6-311+g(2d,p) level of theory. The diagram illustrates that there are no intersections between the surfaces. Thus, the only possible reaction of Mg with O_2(a) is recombination to $MgO_2(^1A_1)$.

Figure 10 illustrates the singlet and triplet potential energy surfaces for reaction 4, SiO + O_2(a). This reaction should be extremely slow, for several reasons: (1), a barrier in the entrance channel of 9 kJ mol^{-1}; (b) a barrier of 55 kJ mol^{-1} in the exit channel to SiO_2 + $O(^3P)$; (c) and the requirement to hop from the reactant singlet electronic surface onto the product triplet surface. Thus reaction 4 will not be competitive with the reaction SiO + O_3 [*Gomez Martin et al.*, 2009b] as a route for oxidising SiO to SiO_2 in the MLT.

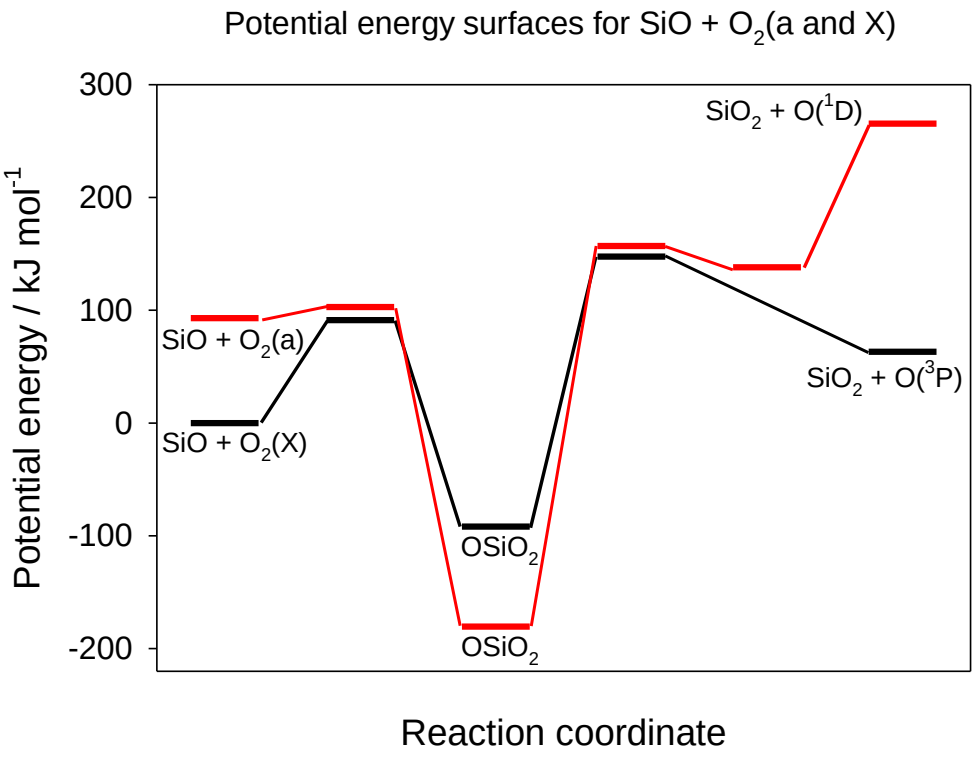

Figure 10. Potential energy curves (calculated at the B3LYP/6-311+g(2d,p) level of theory) for the singlet surface (red lines) and triplet surface (black lines). Note that there is a barrier of 10 kJ mol^{-1} on the singlet surface which will slow recombination to $OSiO_2$. Formation of SiO_2 + O would require both surface crossing and overcoming a significant barrier of 55 kJ mol^{-1}.

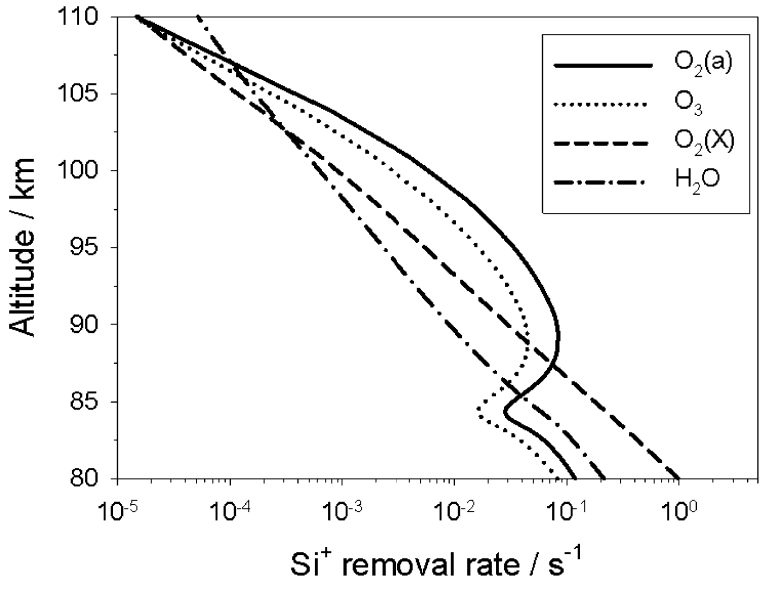

Figure 11. Vertical profiles in the mesosphere/lower thermosphere of the first-order removal rates of Si^+. Note that the major daytime removal process between 85 and 107 km is by reaction with O_2(a). Conditions are 40°N, April at midday.

Atmospheric modelling

The geophysical significance of these reactions was tested using output from the Whole Atmosphere Chemistry Climate Model (WACCM), which is a state-of-the-art atmospheric chemistry climate model coupled with a detailed chemistry scheme (http://waccm.acd.ucar.edu/). The only reactions studied in this project which are atmospherically important are reactions 1 and 5. Figure 11 shows the vertical profile in the MLT of the first-order removal rates of Si^+ by a number of reactions. During daytime, when $[O_2(a)]$ is about 30 times larger than $[O_3]$, reaction 5 is the most important removal process for Si^+. Between 85 and 105 km, the rate of reaction 5 is roughly double that of the reaction $Si^+ + O_3$ [*Eyet et al.*, 2010]. In the case of reaction 1, the order is reversed: the rate of Ca + O_3 [*Helmer et al.*, 1993] is roughly four times faster than reaction 1, during daytime between 80 and 110 km.

Conclusions

This was a successful project in which all major objectives were achieved. As explained above, it was decided to replace a study of Si + $O_2(a)$ with a study of the Mg atom reaction, both because this was experimentally tractable (Mg does reacts very slowly with ground state $O_2(X)$, whereas the Si reaction is close to the collision frequency), and because the Mg reaction provided an illuminating contrast to Ca + $O_2(a)$. Although it turned out that the atmospheric significance of these reactions was limited, they have proved to be of fundamental interest as a test for advanced quantum chemistry calculations and rate theory.

References

Bardeen, C. G., O. B. Toon, E. J. Jensen, D. R. Marsh, and V. L. Harvey (2008), Numerical simulations of the three-dimensional distribution of meteoric dust in the mesosphere and upper stratosphere, *J. Geophys. Res.-Atmos.*, *113*(D17), article no.: D17202.

Batista, P. P., H. Takahashi, B. R. Clemesha, and E. J. Llewellyn (1996), Mesospheric ozone concentration at an equatorial location from the 1.27-micron O_2 airglow emission, *J. Geophys. Res.-Atmos.*, *101*(A4), 7917-7921.

Bowman, M. R., A. J. Gibson, and M. C. W. Sandford (1969), Atmospheric sodium measured by a tuned laser radar, *Nature*, *221*, 456-457.

Brasseur, G. P., and S. Solomon (2005), *Aeronomy of the Middle Atmosphere*, Springer, Dordrecht.

Broadley, S. L., T. Vondrak, and J. M. C. Plane (2007), A kinetic study of the reactions of Ca+ ions with O_3, O_2, N_2, CO_2 and H_2O, *Phys. Chem. Chem. Phys.*, *9*(31), 4357-4369.

Campbell, M. L., and J. M. C. Plane (2001), Kinetic study of the gas-phase reaction of $Ca(^1S)$ with O_2 from 296 to 623 K, *J. Phys. Chem. A*, *105*(14), 3515-3520.

Eska, V., U. von Zahn, and J. M. C. Plane (1999), The terrestrial potassium layer (75-110 km) between 71°S and 54°N: Observations and modeling, *J. Geophys. Res.-Atmos.*, *104*(A8), 17173-17186.

Eyet, N., R. J. Bemish, A. A. Viggiano, and J. M. C. Plane (2010), Mesospheric implications for the reaction of Si^+ with $O_2(a\ ^1\Delta_g)$, *Geophys. Res. Lett.*, *37*, art. no.: L20801.

Fan, Z. Y., J. M. C. Plane, J. Gumbel, J. Stegman, and E. J. Llewellyn (2007), Satellite measurements of the global mesospheric sodium layer, *Atmos. Chem. Phys.*, *7*, 4107-4115.

Frisch, M. J., G. W. Trucks, H. B. Schlegel, G. E. Scuseria, M. A. Robb, J. R. Cheeseman, G. Scalmani, V. Barone, B. Mennucci, G. A. Petersson, H. Nakatsuji, M. Caricato, X. Li, H. P.

Hratchian, A. F. Izmaylov, J. Bloino, G. Zheng, J. L. Sonnenberg, M. Hada, M. Ehara, K. Toyota, R. Fukuda, J. Hasegawa, M. Ishida, T. Nakajima, Y. Honda, O. Kitao, H. Nakai, T. Vreven, J. J. A. Montgomery, J. E. Peralta, F. Ogliaro, M. Bearpark, J. J. Heyd, E. Brothers, K. N. Kudin, V. N. Staroverov, R. Kobayashi, J. Normand, K. Raghavachari, A. Rendell, J. C. Burant, S. S. Iyengar, J. Tomasi, M. Cossi, N. Rega, J. M. Millam, M. Klene, J. E. Knox, J. B. Cross, V. Bakken, C. Adamo, J. Jaramillo, R. Gomperts, R. E. Stratmann, O. Yazyev, A. J. Austin, R. Cammi, C. Pomelli, J. W. Ochterski, R. L. Martin, K. Morokuma, V. G. Zakrzewski, G. A. Voth, P. Salvador, J. J. Dannenberg, S. Dapprich, A. D. Daniels, O. Farkas, J. B. Foresman, J. V. Ortiz, J. Cioslowski, and D. J. Fox (2009), *Gaussian 09, Revision A.1*, Gaussian, Inc., Wallingford CT.

Gardner, C. S., J. M. C. Plane, W. L. Pan, T. Vondrak, B. J. Murray, and X. Z. Chu (2005), Seasonal variations of the Na and Fe layers at the South Pole and their implications for the chemistry and general circulation of the polar mesosphere, *J. Geophys. Res.-Atmos.*, *110*(D10), article no.: D1030210.

Gerding, M., M. Alpers, U. von Zahn, R. J. Rollason, and J. M. C. Plane (2000), Atmospheric Ca and Ca^+ layers: Midlatitude observations and modeling, *J. Geophys. Res-Space Phys.*, *105*(A12), 27131-27146.

Gomez Martin, J. C., M. Blitz, and J. M. C. Plane (2009a), Kinetic studies of atmospherically relevant silicon chemistry. Part 1: Silicon atom reactions, *Phys. Chem. Chem. Phys.*, *4*, 671-678.

Gomez Martin, J. C., M. A. Blitz, and J. M. C. Plane (2009b), Kinetic studies of atmospherically relevant silicon chemistry. Part II: silicon monoxide reactions, *Phys. Chem. Chem. Phys.*, *11*, 10945-10954.

Grebowsky, J. M., and A. C. Aikin (2002), In situ measurements of meteoric ions, in *Meteors in the earth's atmosphere*, edited by E. Murad and I. P. Williams, pp. 189-214, Cambridge University Press, Cambridge.

Helmer, M., J. M. C. Plane, and M. R. Allen (1993), A Kinetic Investigation of the Reaction Ca + O_3 over the Temperature-Range 213 K - 383 K, *Journal of the Chemical Society-Faraday Transactions*, *89*(5), 763-769.

Helmer, M., and J. M. C. Plane (1994a), Experimental and Theoretical Study of the Reaction $Fe+O_2+N_2$ --> FeO_2+N_2, *J. Chem. Soc.-Faraday Trans.*, *90*(3), 395-401.

Helmer, M., and J. M. C. Plane (1994b), Kinetic-Study of the Reaction between Fe and O_3, under Mesospheric Conditions, *J. Chem. Soc.-Faraday Trans.*, *90*(1), 31-37.

Hunten, D. M., R. P. Turco, and O. B. Toon (1980), Smoke and dust particles of meteoric origin in the mesosphere and stratosphere, *J. Atmos. Sci.*, *37*, 1342-1357.

Kalashnikova, O., M. Horanyi, G. E. Thomas, and O. B. Toon (2000), Meteoric Smoke production in the atmosphere, *Geophys. Res. Lett.*, *27*, 3293-3296.

Kane, T. J., and C. S. Gardner (1993), Structure and Seasonal Variability of the Nighttime Mesospheric Fe Layer at Midlatitudes, *J. Geophys. Res.-Atmos.*, *98*(D9), 16875-16886.

Kopp, E. (1997), On the abundance of metal ions in the lower ionosphere, *J. Geophys. Res.-Atmos.*, *102*(A5), 9667-9674.

Lide, D. R. (2006), *Handbook of Physics and Chemistry*, CRC Press, Boca Raton, FL.

Megner, L., M. Rapp, and J. Gumbel (2006), Distribution of meteoric smoke - sensitivity to microphysical properties and atmospheric conditions, *Atmos. Chem. Phys.*, *6*, 4415-4426.

Midey, A., I. Dotan, and A. A. Viggiano (2008), Temperature Dependences for the Reactions of O^- and O_2^- with $O_2(a^1\Delta_g)$ from 200 to 700 K, *J. Phys. Chem. A*, *112*, 3040–3045.

Midey, A. J., I. Dotan, S. Lee, W. T. Rawlins, M. A. Johnson, and A. A. Viggiano (2007), Kinetics for the Reactions of O^- and O_2^- with $O_2(a\ ^1\Delta_g)$ Measured in a Selected Ion Flow Tube at 300 K, *J. Phys. Chem. A.*, *111*, 5218-5222.

Midey, A. J., I. Dotan, J. V. Seeley, and A. A. Viggiano (2009), Reactions of Small Negative Ions with $O_2(a\ ^1\Delta_g)$ and $O_2(X\ ^3\Sigma_g^-)$ *Int. J. Mass Spectrom., 280*, 6-11.

Mitchell, S. A., and P. A. Hackett (1990), Visible multiphoton dissociation of $Fe(CO)_5$ for production of iron atoms, *J. Chem. Phys.*, ***93***, 7813-7821.

Nien, C. F., B. Rajasekhar, and J. M. C. Plane (1993), Unusual Kinetic-Behavior of the Reactions $Mg+O_2+M$ and $Ca+O_2+M$ ($M=N_2$,He) over Extended Temperature Ranges, *J. Phys. Chem.*, *97*(47), 12422-12422.

Plane, J. M. C. (2003), Atmospheric chemistry of meteoric metals, *Chem. Rev.*, *103*(12), 4963-4984.

Plane, J. M. C., B. J. Murray, X. Z. Chu, and C. S. Gardner (2004), Removal of meteoric iron on polar mesospheric clouds, *Science*, *304*(5669), 426-428.

Saunders, R. W., and J. M. C. Plane (2006), A laboratory study of meteor smoke analogues: Composition, optical properties and growth kinetics, *J. Atmos. Solar-Terr. Phys.*, *68*(18), 2182-2202.

Scharringhausen, M., A. C. Aikin, J. P. Burrows, and M. Sinnhuber (2008), Global column density retrievals of mesospheric and thermospheric MgI and MgII from SCIAMACHY limb and nadir radiance data, *J. Geophys. Res-Space Phys.*, *113*(D13), article no.: D13303.

Self, D. E., and J. M. C. Plane (2003), A kinetic study of the reactions of iron oxides and hydroxides relevant to the chemistry of iron in the upper atmosphere, *Phys. Chem. Chem. Phys.*, *5*, 1407-1418.

Shettle, E. P., M. T. DeLand, G. E. Thomas, and J. J. Olivero (2009), Long term variation in the frequency of polar mesospheric clouds in the Northern Hemisphere from SBUV, *Geophys. Res. Lett.*, *36*, article no.: L02803.

Vondrak, T., J. M. C. Plane, S. L. Broadley, and D. Janches (2008), A chemical model of meteoric ablation, *Atmos. Chem. Phys.*, *8*, 1-17.

Woodcock, K. R. S., T. Vondrak, S. R. Meech, and J. M. C. Plane (2006), A kinetic study of the reactions $FeO^+ + O$, $Fe^+.N_2 + O$, $Fe^+.O_2 + O$ and $FeO^+ + CO$: implications for sporadic E layers in the upper atmosphere, *Phys. Chem. Chem. Phys.*, *8*(15), 1812-1821.